GeoConvention 2015
GEOSCIENCE
new horizons
Telus Convention Centre • 4-8 May 2015 • Calgary, AB Canada

Estimation of the Elastic Constants for HTI Media Using Full-Newton Multi-parameter Full Waveform Inversion

Wenyong Pan, Kris Innanen, Gary Margrave, CREWES Project, University of Calgary*
Mike Fehler, Xinding Fang, ERL, Massachusetts Institute of Technology
and Junxiao Li, CREWES Project, University of Calgary

Summary

We use the Full-Newton multi-parameter full waveform inversion method to determine the elastic constants of an HTI medium. We explain the physical meaning of the first-order and second-order terms in the multi-parameter Hessian and propose to calculate the second-order term by using a backpropagation technique with a multi-parameter second-order virtual source. The Full-Newton method has a better convergence rate than the Gauss-Newton method because it suppresses the artifacts caused by the second-order scattered energy in the data residuals, which is verified using a 2D HTI numerical example.

Introduction

In recent years, the full waveform inversion (FWI) method has become popular for estimating subsurface parameters (Tarantola, 1984; Virieux and Operto, 2009; Warner et al., 2013; Margrave et al., 2011; Margrave et al., 2010). The method uses full wavefield information during the inversion by iteratively minimizing the difference between the modelled and observed data. FWI can also be used to estimate fracture properties when fractured reservoirs are considered as equivalent anisotropic media. We focus on inverting for the elastic constants in HTI media using Full-Newton multi-parameter FWI.

In mono-parameter FWI, the steepest-descent methods ignore the Hessian preconditioner resulting in a blurred and poorly-scaled update. The Hessian operator acts as a deconvolution operator to compensate for geometrical spreading at each image point, to de-blur the gradient and to suppress the second-order scattering effects (Pratt et al., 1998; Pan et al., 2014; Pan et al., 2014a, 2014b). Inverting for multiple parameters using multi-parameter FWI is more challenging. The gradient-based updates in multi-parameter FWI also suffer from the cross-talk problem caused by the coupling effects of the different physical parameters (Operto et al., 2013; Innanen, 2014a, 2014b). The off-diagonal blocks of the multi-parameter approximate Hessian indicate the correlation of partial derivative wavefields with respect to two different physical parameters, which can mitigate the cross-talk phenomena for multi-parameter FWI.

The gradient is also contaminated by the second-order scattered energy in the data residuals. Pratt et al. (1998) discussed the second-order term in the mono-parameter full Hessian, which accounts for the second-order scattering effects, can be calculated by correlation between the second-order partial derivative wavefields with the data residuals. The second-order term in the mono-parameter Hessian can also be calculated using a backpropagation technique (Fichtner and Trampert, 2011). The second-order term in multi-parameter Hessian becomes more complex and the second-order partial derivative wavefields may be caused by the perturbations of more than one physical parameter. Incorporating these second-order terms for preconditioning the gradient can eliminate the second-order scattering effects in the gradient. What's more, the adjoint sate method can also be employed for calculating the second-order term. In this paper, we first, analyze the roles of the first-order and second-order terms in multi-parameter FWI with a 2D HTI case. Then, we focus on calculating the second-order term in multi-parameter full Hessian and apply the Full-Newton multi-parameter FWI for elastic constant inversion in HTI media.

Theory and Method

In this section, we will illustrate the multi-parameter update using a 2D HTI model, which can be described by 4 elastic constants (c_{33}, c_{55}, c_{11} and c_{13}). Thus, the model perturbation vector in multi-parameter Full-Newton FWI can be expressed as:

$$\mathbf{\delta m}(\mathbf{r}) = \sum_{\mathbf{r}'} \mathbf{H}^{-1}(\mathbf{r},\mathbf{r}')\mathbf{g}(\mathbf{r}'), \tag{1}$$

where $\mathbf{r}=(x,\ y=0,\ z)$ indicates the position of the model parameter, the model perturbation vector $\mathbf{\delta m}$ and gradient vector $\mathbf{g}$ consist of 4 elements corresponding to the 4 elastic constants:

$$\mathbf{\delta m}(\mathbf{r}) = \left[\delta c_{33}(\mathbf{r}), \delta c_{55}(\mathbf{r}), \delta c_{11}(\mathbf{r}), \delta c_{13}(\mathbf{r})\right]^{\dagger}, \quad \mathbf{g}(\mathbf{r}') = \left[g_{33}(\mathbf{r}'), g_{55}(\mathbf{r}'), g_{11}(\mathbf{r}'), g_{13}(\mathbf{r}')\right]^{\dagger}, \tag{2}$$

where the symbol "†" means transpose. The full Hessian matrix $\mathbf{H}$ has 4 diagonal blocks corresponding to the second-order partial derivative of the misfit function with respect to the same physical parameter and 12 off-diagonal blocks corresponding to the second-order partial derivative of the misfit function with respect to two different physical parameters. It can be expressed as:

$$\mathbf{H}=\begin{bmatrix} \mathbf{H}_{3333} & \mathbf{H}_{3355} & \mathbf{H}_{3311} & \mathbf{H}_{3313} \\ \mathbf{H}_{5533} & \mathbf{H}_{5555} & \mathbf{H}_{5511} & \mathbf{H}_{5513} \\ \mathbf{H}_{1133} & \mathbf{H}_{1155} & \mathbf{H}_{1111} & \mathbf{H}_{1113} \\ \mathbf{H}_{1333} & \mathbf{H}_{1355} & \mathbf{H}_{1311} & \mathbf{H}_{1313} \end{bmatrix}. \tag{3}$$

The full Hessian $\mathbf{H}$ can be written as the summation of the first-order term $\tilde{\mathbf{H}}$ (approximate Hessian) and a second-order term $\bar{\mathbf{H}}$:

$$\mathbf{H}=\tilde{\mathbf{H}}+\bar{\mathbf{H}}. \tag{4}$$

Each element in the approximate Hessian is the correlation of two first-order partial derivative wavefields and the each element in the second-order term $\bar{\mathbf{H}}$ is the correlation of second-order partial derivative wavefields with the data residuals. For example, the element $\tilde{H}_{3355}(\mathbf{r}, \mathbf{r}')$ in the off-diagonal block matrix $\tilde{\mathbf{H}}_{3355}$ and the element $\bar{H}_{3355}(\mathbf{r}, \mathbf{r}')$ in the off-diagonal block matrix $\bar{\mathbf{H}}_{3355}$ can be expressed as:

$$\tilde{H}_{3355}(\mathbf{r}, \mathbf{r}') = \frac{\partial \mathbf{u}^{\dagger}}{\partial c_{33}(\mathbf{r})}\frac{\partial \mathbf{u}^{*}}{\partial c_{55}(\mathbf{r}')}, \bar{H}_{3355}(\mathbf{r}, \mathbf{r}') = \frac{\partial^2 \mathbf{u}^{\dagger}}{\partial c_{33}(\mathbf{r})\partial c_{55}(\mathbf{r}')}\Delta \mathbf{d}^{*}, \tag{5}$$

where the symbol "*" means complex conjugate and $\Delta\mathbf{d}$ is the data residual vector. The element $\tilde{H}_{3355}(\mathbf{r}, \mathbf{r}')$ is the correlation of the first-order partial derivative wavefields due to δc_{33} at $\mathbf{r}$ with the first-order partial derivative wavefields due to δc_{55} at $\mathbf{r}'$. $\frac{\partial^2 \mathbf{u}^{\dagger}}{\partial c_{33}(\mathbf{r})\partial c_{55}(\mathbf{r}')}$ indicates the second-order partial derivative wavefields and it is formed when the first-order partial derivative wavefields due to δc_{33} at $\mathbf{r}$ is second-order scattered due to δc_{55} at $\mathbf{r}'$. To calculate the second-order term in the multi-parameter Hessian, a total of $(N_p N_m)^2/2$ forward modelling problems need to be solved, where N_m is the number of node points and N_p is the number of physical parameters assigned to describe each node. To reduce this computational burden, consider the first-order partial derivative wavefields due to $\delta m_i(\mathbf{r})$:

$$\frac{\partial \mathbf{u}}{\partial m_i(\mathbf{r})} = -\mathbf{L}^{-1}\frac{\partial \mathbf{L}}{\partial m_i(\mathbf{r})}\mathbf{u}, \tag{6}$$

where $\mathbf{L}$ is the impedance matrix, i indicates the physical parameter type, and the interaction of the background wavefields with the model perturbation serves as the first-order virtual source $\tilde{\mathbf{f}} = -\frac{\partial \mathbf{L}}{\partial m_i(\mathbf{r})}\mathbf{u}$.

Taking partial derivative with respect to $m_j(\mathbf{r}')$ on both sides of equation (6) forms the multi-parameter second-order partial derivative wavefields:

$$\frac{\partial^2 \mathbf{u}}{\partial m_i(\mathbf{r})\partial m_j(\mathbf{r}')} = \mathbf{L}^{-1}\left(-\frac{\partial \mathbf{L}}{\partial m_i(\mathbf{r})}\frac{\partial \mathbf{u}}{\partial m_j(\mathbf{r}')} - \frac{\partial \mathbf{L}}{\partial m_j(\mathbf{r}')}\frac{\partial \mathbf{u}}{\partial m_i(\mathbf{r})} - \frac{\partial^2 \mathbf{L}}{\partial m_i(\mathbf{r})\partial m_j(\mathbf{r}')}\mathbf{u}\right), \tag{7}$$

where m_j means physical parameter different from m_i. We can then substitute equation (7) into the second-order term $\bar{\mathbf{H}}$. For example, element $\bar{H}_{3355}(\mathbf{r}, \mathbf{r}')$ in equation (5) becomes:

$$\bar{H}_{3355}(\mathbf{r}, \mathbf{r}') = \tilde{\tilde{\mathbf{f}}}_{3355}^{\dagger}(\mathbf{L}^{-1})^{\dagger}\Delta\mathbf{d}^{*}, \tag{8}$$

where $\tilde{\tilde{\mathbf{f}}}_{3355}$ means the second-order multi-parameter virtual source due to δc_{33} and δc_{55}. Thus, the second-order term in the multi-parameter Hessian can also be constructed using the adjoint state technique and the computational cost is reduced to $2N_pN_m$.

Examples

In this section, we first give a numerical example to illustrate the multi-parameter Hessian. The 2D HTI model is a 30x30 model with grid size of 5 m in both horizontal and vertical dimensions and 4 elastic constants (c_{33}, c_{55}, c_{11} and c_{13}) are used to describe each node. The initial model is elastic and isotropic with elastic constants $c_{33} = 14.06\text{GPa}$, $c_{55} = 6.32\text{GPa}$, $c_{11} = 14.06\text{GPa}$ and $c_{13} = 1.42\text{GPa}$ (density $\rho = 2.0\text{g/cm}^3$).

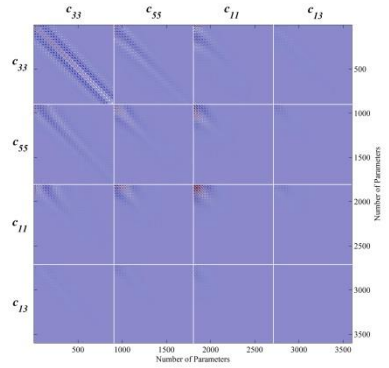

Figure 1. The multi-parameter approximate Hessian $\tilde{\mathbf{H}}$ for the 4 elastic constants.

Figure 1 shows the multi-parameter approximate Hessian $\tilde{\mathbf{H}}$ for elastic constants c_{33}, c_{55}, c_{11} and c_{13}. We can see that the multi-parameter approximate Hessian is a 3600x3600 square and symmetric matrix. It has 4 diagonal blocks and 12 off-diagonal blocks and each block is a 900x900 square matrix. We can see that the multi-parameter approximate Hessian is banded due to finite frequency effects and the diagonal block $\tilde{\mathbf{H}}_{3333}$ dominates the matrix. This is because c_{33} directly relates to P-wave velocity and the first-order partial derivative wavefields recorded at the top surface caused by δc_{33} is much stronger than those due to other elastic constants. The stronger amplitudes in the off-diagonal blocks means the stronger cross-talk between different physical parameters.

Figure 2 shows the multi-parameter full Hessian plotted in model space. Figures 2a, b, c and d show the 555th row in the diagonal blocks $\tilde{\mathbf{H}}_{3333}$, $\tilde{\mathbf{H}}_{5555}$, $\tilde{\mathbf{H}}_{1111}$ and $\tilde{\mathbf{H}}_{1313}$ of the multi-parameter Hessian. Figures 2 e, f and g show the show the 555th row in the off-diagonal blocks $\tilde{\mathbf{H}}_{3355}$, $\tilde{\mathbf{H}}_{3311}$ and $\tilde{\mathbf{H}}_{3313}$. Figures 2 h, i, j and k show the 555th row in the diagonal blocks $\bar{\mathbf{H}}_{3333}$, $\bar{\mathbf{H}}_{5555}$, $\bar{\mathbf{H}}_{1111}$ and $\bar{\mathbf{H}}_{1313}$ of the second-order term. Figures 2l, m and n show the 555th row in the off-diagonal blocks $\bar{\mathbf{H}}_{3355}$, $\bar{\mathbf{H}}_{3311}$ and $\bar{\mathbf{H}}_{3313}$ of the second-order term. Figures 3a, b and c show the model perturbations for elastic constants for c_{33} with first-order term preconditioning when increasing the model perturbations from 10% to 20% and 30%. Figures 3d, e

and f show the model perturbations for elastic constants for c_{55} with first-order term preconditioning when increasing the model perturbations from 10% to 20% and 30%. We can see that with increasing model errors, the artifacts caused by second-order scattered energy become more obvious.

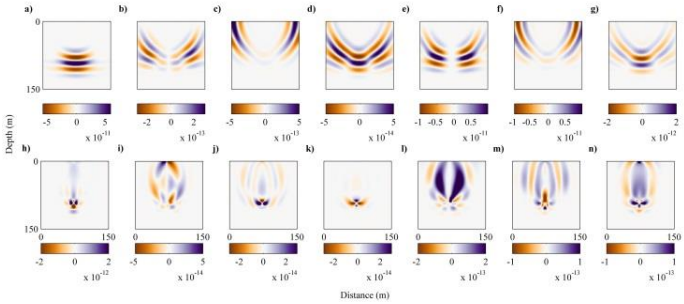

Figure 2. The first-order and second-order terms in the multi-parameter full Hessian plotted in model space.

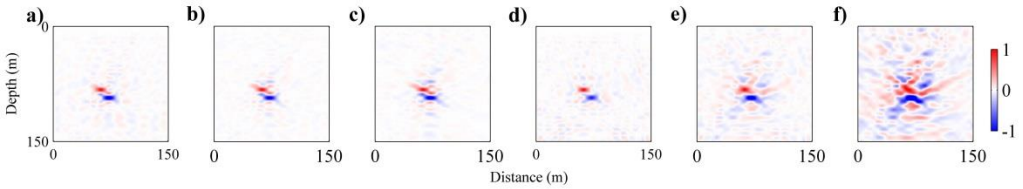

Figure 3. The estimated model perturbations contaminated by second-order scattering effects.

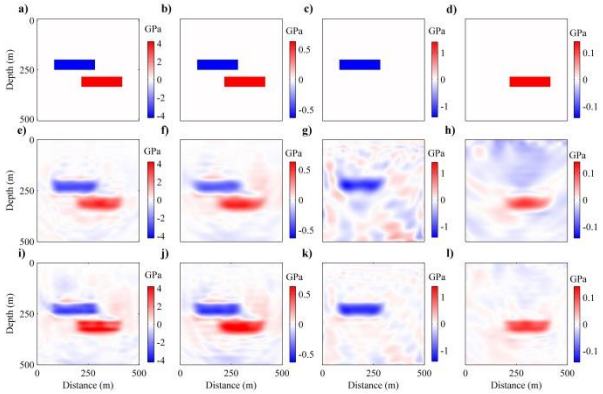

Figure 4. The estimated elastic constants perturbations using Gauss and Full-Newton multi-parameter FWI.

We then apply the Gauss-Newton and Full-Newton multi-parameter FWI on a more complex model. Figures 4a, b, c and d show the true perturbations for elastic constants c_{33}, c_{55}, c_{11} and c_{13}. Figures 4e, f, g and h show the estimated model perturbations for different elastic constants using Gauss-Newton multi-parameter FWI after 10 iterations. Figures 4i, j, k and l show the estimated model perturbations using Full-Newton multi-parameter FWI iterations. It can be seen that the Full-Newton method can estimate the model perturbations better for incorporating the second-order term in the multi-parameter Hessian.

Conclusions

We have incorporated the second-order term in multi-parameter full Hessian is for inverting for the elastic constants in HTI media. Compared to the Gauss-Newton method, the Full-Newton method can estimate the model perturbations more efficiently by suppressing the multi-parameter second-order scattering effects.

Acknowledgements

This work was funded by CREWES sponsors and NSERC (Natural Science and Engineering Research Council of Canada) through the grant CRDPJ 379744-08.

References

Fichtner, A. and J. Trampert, 2011, Hessian kernels of seismic data functionals based upon adjoint techniques: Geophysical Journal International, **185**, 775-798.

Innanen, K. A., 2014a, Seismic AVO and the inverse Hessian in precritical reflection full waveform inversion: Geophysical Journal International, **199**, 717-734.

Innanen, K. A., 2014b, Reconciling seismic avo and precritical reflection FWI-analysis of the inverse Hessian: SEG Expanded Abstracts, 1022-1027.

Margrave, G. F., R. J. Ferguson, and C. M. Hogan, 2011, Full-waveform inversion using wave-equation depth migration with tying to wells: 81st Annual International Meeting, SEG Expanded Abstracts, 2454–2458.

Margrave, G. F., R. J. Ferguson, and C. M. Hogan, 2010, Full-waveform inversion with wave equation migration and well control: CREWES Annual Report.

Operto, S., Y. Gholami, V. Prieux, A. Ribodetti, R. Brossier, L. Metivier and J. Virieux, 2013, A guided tour of multiparameter full-waveform inversion with multicomponent data: from theory to practice: The Leading Edge, 1040-1054.

Pan, W., G. F. Margrave, and K. A. Innanen, 2014, Iterative modelling migration and inversion (immi): Combining full waveform inversion with standard inversion methodology: SEG Expanded Abstracts, 938-943, doi: 10.1190/segam2014-0402.1.

Pan, W., K. A. Innanen and G. F. Margrave, 2014a, A comparison of different scaling methods for least-squares migration/inversion: EAGE Expanded Abstracts, doi: 10.3997/2214-4609.20141164.

Pan, W., K. A. Innanen and G. F. Margrave, 2014b, Efficient t-p domain waveform inversion, Part 2: Sensitivity to p component setting, source spacing and noise: SEG Expanded Abstracts, 1110-1115, 10.1190/segam2014-0773.1.

Pratt, R. G., C. Shin, and G. J. Hicks, 1998, Gauss-newton and full newton methods in frequency-space seismic waveform inversion: Geophysical Journal International, **133**, 341-362.

Tarantola , A., 1984, Inversion of seismic reflection data in the acoustic approximation: Geophysics, 49, 1259–1266.

Virieux, A. and S. Operto, 2009, An overview of full-waveform inversion in exploration geophysics: Geophysics, **74**, WCC1-WCC26.

Warner, M., A. Ratclie, T. Nangoo, J. Morgan, A. Umpleby, N. Shah, V. Vinje, I. Stekl, L. Guasch, C. Win, G. Gonroy, and A. Bertrand, 2013, Anisotropic 3D full-waveform inversion: Geophysics, **78**, R59-R80.